Journal of Applied Electrochemistry **33**: 709–715, 2003.

AISI 304 L stainless steel decontamination by a corrosion process using cerium IV regenerated by ozone
Part II: Process optimization

J.P. CAIRE[1], S. CULLIE[1], F. DALARD[1], J.M. FULCONIS[2] and H. DELAGRANGE[2]
[1]*LEPMI, ENSEEG, UMR 5631 INPG – CNRS, 1130 Rue de la Piscine, 38402 Saint-Martin d'Hères, France*
[2]*CEA Valrho, BP 171, 30207 Bagnols sur Cèze, France*
*(*author for correspondence, e-mail: jean-pierre.caire@lepmi.inpg.fr)*

Received 8 January 2001; accepted in revised form 21 March 2003

Key words: cerium, corrosion, decontamination, design of experiments, modelling, RSM, ozone

Abstract

Empirical and analytical approaches were used to model a pre-industrial pilot reactor to optimise a new decontamination process for AISI 304 L stainless steel. The alloy corrosion rate was modelled as an analytical function of the total cerium content and the ozone flow injected in the reactor. The empirical model of the corrosion rate, obtained by gravimetry, takes into account all the parameters, including the kinetics of alloy grains detached from the metal by intergranular corrosion. The discrepancy observed between the analytical and empirical models was explained by a two-step corrosion process. The dimensions and quantity of grains falling in the liquid were at first both underestimated. The study showed that the grains had to be extracted continuously from recirculating liquid in the future industrial reactor.

1. Introduction

Part I showed the feasibility of the accelerated corrosion process for AISI 304 L decontamination. In fact, the yield was very low since only 3.5% of the ozone produced was actually used for cerium regeneration in the reactor. It was shown that the process yield depended on both the Ce^{4+} concentration and the regenerative ozone flow (Part I). Moreover, the phenomena involved in the bubble reactor (Figure 1) had to be carefully modelled before any attempt could be made to optimize the micropilot and the process.

Numerous papers have been devoted to the modelling of gas/liquid mass transfer in counter-flow bubble columns similar to ours. Whitman et al. [1] developed the double layer concept to determine the gas quantity transferred in the liquid phase. Mass transfer can be described by the dimensionless Hatta number and the acceleration factor in bubble column reactors [2]. Wang [2] recently modelled the performances of counter-flow reactors by the combined use of hydrodynamic data related to the system of interest (Re_{gas}, Re_{liquid}, Re_{bubble}, a_g) and mass transfer coefficients (k_{la}, k_{lm}). Complex studies of this type were not performed here since the focus was placed on modeling the corrosion process rather than the hydrodynamics of the micropilot reactor.

In the present study, a combination of analytical and empirical models was used to improve knowledge of the process and optimize process yield. The empirical model was established by use of 'design of experiments' (DOE) methodology and the optimization was achieved with the 'response surface methodology' (RSM) [3].

2. Design of experiments

The DOE methodology [3] is based on the statistical processing of responses obtained from a set of carefully chosen experiments for which numerous parameters are varied simultaneously. The set of variables used in the DOE methodology must be independent control parameters. The first step in applying the methodology to our study was therefore to choose the influent parameters and their related domain of interest.

2.1. *Choice of DOE parameters*

Part I demonstrated that the corrosion rate depends mainly on the cerium concentration in the nitric acid solution. Since the Ce^{4+} ions would be rapidly consumed without any regeneration by ozone, ozone mass flow is also an important parameter. A reasonable experimental domain must also be determined. A brief discussion of these choices is presented:

(i) Ce^{4+} concentration controls the corrosion rate. Tests (not described here) showed that a cerium concentration varying between 5×10^{-3} mol l^{-1} and 10^{-2} mol l^{-1} was a convenient domain. The

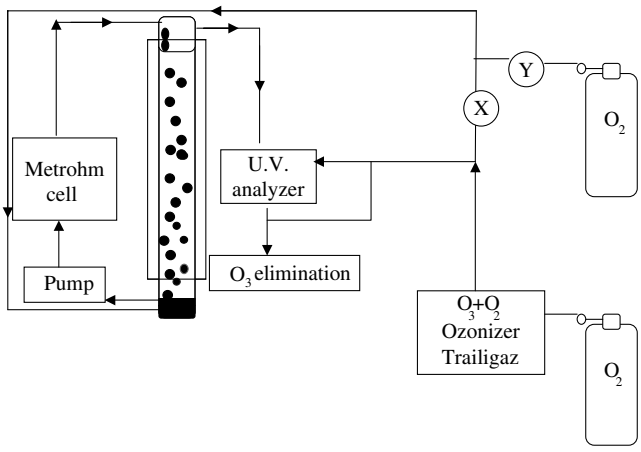

Fig. 1. Metrohm electrochemical cell and pilot reactor (X,Y mass flow controllers).

associated parameter is named Ce in the following screen copies.

(ii) Ozone is the agent of cerium (IV) regeneration. The mass balances proved that ozone was in large excess in the reactor. Ozone concentration must obviously be taken into account, but preliminary pilot tests showed that it could vary widely. The domain of interest of the ozone mass flow was defined between 0.06 and 6 g h^{-1} for practical reasons. Such a variation spanning two decades could have led to a 'lack-of-fit' error [4]. Thus, the DOE was designed by use of the mass flow logarithm (parameter LO3) rather than the mass flow itself.

(iii) The flow of the oxidizing solution (parameter Q_{liq}) is involved on both the diffusion layers at metal–liquid interface and gas/liquid mass transfer. The recycled flow was chosen to vary between 20 and 40 l h^{-1}.

(iv) The incoming flow of oxygen–ozone mixture is known to influence the corrosion rate. However, this parameter had to be set at 60 l h^{-1} for practical reasons.

(v) The solution temperature was set at 25 °C to obtain a low-cost process in an industrial context.

Only parameters (i), (ii) and (iii) were therefore taken into account in this study, leading to a simple, low-cost experimental design.

2.2. *Choice of DOE responses*

To achieve the goals described in Section 2.1, the following four responses of interest were chosen:

(a) The corrosion rate of AISI 304 L measured by weight loss on the corroded specimen (response m_{meas}).

(b) The solution potential $E_{i=0}$ measured with the precious metal electrode. This potential response is representative of Ce^{4+} regeneration by ozone.

(c) Potential difference between the oxidising solution and AISI 304 L (response D_{dp}) which is a good indicator of the oxidation efficiency of metal corrosion by the solution.

(d) The mean corrosion current density (response i_{cor}) which expresses the reaction rate between Ce^{4+} and AISI 304 L alloy.

2.3. *Objectives of DOE methodology with a view to process optimization*

The goals mentioned earlier were then interpreted in the context of future process optimization. For industrial purposes, the target AISI 304 L alloy corrosion rate was set at 0.21 μm h^{-1}. The initial solution potential $E_{i=0}$ could be easily measured using a precious metal electrode. For practical process control purposes, the average corrosion current density had to be modelled by a low-cost system for measuring solution potential.

2.4. *Design of experiments*

Since we used a response surface methodology [3] for optimization purposes, we created a 'central composite in a sphere' (CCI) design using Echip6 [4] with the three parameters defined in Section 2.1. This CCI design consisted of 19 runs including five replicates at the centre of the experimental domain. This is one of the best designs commonly used in the context of RSM. The responses were approximated by quadratic polynomials giving a precise description of experimental data in the domain of interest. This representation made it easier to find the overall optimum for combined responses through use of the 'desirability' concept [5]. The polynomial model associated with each response may be written as

$$y = b_o + \sum_{i=1}^{k} b_i + \sum_{i \neq j}^{k} b_{i,j} X_i X_j + \sum_{i=1}^{k} b_{i,i} X_i^2 \qquad (1)$$

This polynomial includes $2k + k(k-1)/2 + 1$ different coefficients for k parameters. The coefficients were obtained by a multilinear regression implemented in the Echip6 code.

The design was randomised to minimize the effect of the systematic experimental error for each response. Table 1 presents the DOE obtained after the randomisation process. The five replicated experiments (runs 6,7,11,14,17) placed at the centre of the experimental domain are defined by $C = 7.5 \times 10^3$, Log(O3) = −1.4, $Q_{liq} = 30$. A standard deviation (SD) coefficient can be computed from the replicate measurements. The SD coefficient, representative of the experimental dispersion, is used for statistical tests [4].

3. Empirical modelling of corrosion rate

The average corrosion current density (response i_{cor}) can be measured easily and was chosen as a DOE response. Since it was possible to develop an analytical model for the corrosion current density, it was interesting to use

Table 1. Randomized design of experiments

Runs	Cerium concentration $\times 10^{-3}$ /mol l^{-1}	Log [O_3] /m^3 h^{-1}	Q_{liq} /l h^{-1}
1	7.5	1.8	30
2	8.943	0.4475	35.774
3	6.057	−3.2175	35.774
4	8.943	0.4475	24.226
5	5	−1.4	30
6	7.5	−1.4	30
7	7.5	−1.4	30
8	7.5	−4.6	30
9	8.943	−3.2175	24.226
10	6.057	0.4475	24.226
11	7.5	−1.4	30
12	10	−1.4	30
13	6.057	−3.2175	24.226
14	7.5	−1.4	30
15	7.5	−1.4	20
16	7.5	−1.4	40
17	7.5	−1.4	30
18	8.943	−3.2175	35.774
19	6.057	0.4475	35.774

the analytical model to compute the total weight loss due to corrosion. This model is also necessary for the control and monitoring aspects of the future reactor. A quadratic polynomial is rapidly computed and can be easily integrated in an on-line regulation algorithm. The model was used as a new response m_{calc} of the previous DOE, in application of the 'computer experiments' concept [6]. We then had two models for the corroded mass, named hereafter m_{calc} and m_{meas}.

3.1. *Analytical model of corrosion rate*

The analytical model of the corrosion rate was a diffusion model based on the following assumptions: (i) Mass transfer related to corrosion reaction was limited by diffusion, that is, i_{cor} was a function of cerium-(IV) Concentration (Fick's law); (ii) Each fluid flow was laminar. This hypothesis might appear surprising in the case of a bubble column but seems justified by the low Reynolds numbers calculated for each phase; (iii) The flows were steady; (iv) Corroded specimens were cylindrical and flow was axial; and (v) The geometry of each piece was not affected during the corrosion process.

The model takes into account the main hydrodynamic parameters of the reactor and corrosion reaction. The reaction may be written as

$$Ce^{3+} \rightarrow Ce^{4+} + e^{-} \tag{2}$$

The current density i_{cor} related to corrosion is directly proportional to the cerium (IV) concentration according to Fick's law [7]:

$$|i_{cor}| = \frac{nFD}{\delta}[Ce^{4+}] \tag{3}$$

where n is the number of electrons exchanged during the reaction (here $n = 1$), F is the faradaic constant, D the diffusion coefficient and δ the diffusion layer thickness (see Equation 15). The mass transfer coefficient between solution and metal is

$$k_d = \frac{D}{\delta} \tag{4}$$

The parameter k_d is related both to the hydrodynamic parameters and to the specimen geometry [1].

In the presence of a two-phase flow, the Reynolds numbers for liquid and gas phase can be calculated using the same generic formula:

$$Re = \frac{\overline{V}d}{v} = \frac{Q_{liq}d}{Av} \tag{5}$$

where v is the dynamic viscosity. Equation 5 gives respective liquid and gas Reynolds numbers of 177 and 84, so that the two-phase flow can be considered laminar. The second hypothesis was validated and these results formed the basis of the choice of correlation used for the k_d computation [1]:

$$\frac{k_d d_h}{D} = 1.614\left(Re_a Sc \frac{d_h}{L}\right)^{1/3} \tag{6}$$

The equivalent hydrodynamic diameter of the test cylinder d_h is obtained from the inner and outer radius:

$$d_h = 2(r_e - r_i) \tag{7}$$

The dimensionless Schmidt number is defined as

$$S_c = \frac{v}{D} \tag{8}$$

The axial Reynolds number associated with the cylinder is

$$Re_a = \frac{2\overline{V}(r_e - r_i)}{v} \tag{9}$$

The flow rate through the area A has the same definition for both phases:

$$\overline{V} = \frac{Q_{liq}}{A} \tag{10}$$

Diffusivity D is known and equal to 6.7×10^{-10} m^2 s^{-1}. Thus, δ can be deduced from k_d and Equation 4.

The model also assumes: (a) that activities of the different species were given by their respective concentrations, and (b) that in the concentration range studied, the potential was only related to the concentration ratio of cerium ions. This hypothesis is justified later. Then, the following equation gives the instantaneous potential of $E(t)$:

$$E(t) = E^{\circ}_{Ce^{4+}/Ce^{3+}} + 2.3\frac{RT}{nF}\log_{10}\left[\frac{Ce^{4+}(t)}{Ce^{3+}(t)}\right] \tag{11}$$

A simple mass balance shows the constancy of total cerium concentration in the solution:

$$[Ce_{total}] = [Ce^{3+}(t)] + [Ce^{4+}(t)] \quad (12)$$

The corrosion current density is computed from the cathodic limiting current:

$$i_{cor}(t) = |i_{lim,C}(t)| \quad (13)$$

The limiting current reads:

$$|i_{lim,C}(t)| = \frac{nFD[Ce^{4+}(t)]}{\delta} \quad (14)$$

The thickness of the boundary layer δ is given by [5]

$$\delta = 1.614\, D^{1/3} v^{1/6} \Omega^{-1/2} \quad (15)$$

The $Ce^{4+}(t)$ instantaneous concentration in solution can be expressed as a function of the solution potential:

$$[Ce^{4+}(t)] = [Ce_{total}] \times \frac{10^p}{1+10^p} \quad (16)$$

where $p = [E(t) - E^{\circ}_{Ce^{4+}/Ce^{3+}}]F/2.3\,RT$.

The instantaneous current density of corrosion $i_{cor}(t)$ is easily deduced from Equations 11 to 16:

$$i_{cor}(t) = 1.614\, \frac{FD}{d_h} \left(\frac{Q_{liq} 2(r_e - r_i) d_h}{\Omega D L} \right)^{1/3} \times \left([Ce_{total}] \times \frac{10^p}{1+10^Q} \right) \quad (17)$$

where $Q = [E(t)_{solution} - E^{\circ}_{Ce^{4+}/Ce^{3+}}]F/2.3\,RT$.

All the terms in Equation 17 are known except the instantaneous potential $E(t)$ which can be easily measured. Integration of the corrosion current density from Equation 17 gives the mean corrosion current density during the experimental time T:

$$\bar{i}_{cor} = \frac{1}{T} \int_0^T i_{cor}(t) \mathrm{d}t \quad (18)$$

The corresponding mass of metal eliminated during the experiment is deduced:

$$m = \frac{\bar{i}_{cor} M_{inox} T}{n_{inox} F} \quad (19)$$

with

$$\frac{M_{inox}}{n_{inox}} = \left(0.70 \frac{M_{Fe}}{3} + 0.18 \frac{M_{Cr}}{6} + 0.10 \frac{M_{Ni}}{2} \right) \quad (20)$$

It should be noted that this computed mass is obviously lower than the mass obtained from experimental data. The model does not take into account the grain unsealing effect, a phenomenon that increases both corroded mass and surface subjected to cerium attack (see Part I).

3.2. *Validation of the numerical model*

First, the mean rest potential of the solution was measured versus time. The previous numerical model of corrosion was then used. The calculations gave a mean corrosion current density of about 5×10^{-5} A cm^{-2}, which is close to the 6×10^{-5} A cm^{-2} obtained in beaker experiments performed with a 0.25 mol l^{-1} cerium concentration. Further validation of the experiments by Equation 17 is given in the next paragraph.

4. Global statistical analysis of results

Table 2 presents the overall results given by the Echip6 software [4] for the four main responses studied in the previously-defined experimental domain. The nine terms of the assumed quadratic model appear in the right column, other columns being devoted to the responses. The number of stars attributed to an individual coefficient of each model results from an analysis of variance (ANOVA) based on the standard deviation (SD) coefficient computed from replicates. The number of stars is related to the probability of nullity calculated for each coefficient. For Echip6, 1, 2 and 3 stars correspond to respective significance levels of 5%, 1% and 0.1%. The absence of stars infers that the corresponding coefficient has no statistical significance. This means that the corresponding parameter has no effect on the response of interest. The probability results are used to disregard the insignificant coefficients and obtain a simpler 'refined' model.

Table 2 shows that the total cerium concentration is the only significant parameter affecting the corrosion rate and current density responses. Such results confirm that cerium is the main agent of corrosion. However, the ozone flow logarithm LO3 has both linear and quadratic effects on the three responses. It should be emphasised that no significant interaction between two

Table 2. Influential parameters for each response of interest

Corrosion rate	Difference of potential	Potential of solution	Current density of corrosion	Influential parameters
***			***	Ce
***	***	***		LO3
			***	Q_{liq}
				Ce*LO3
				Ce*Q_{liq}
				LO3*Q_{liq}
				$(Ce)^2$
***	***	**		$(LO3)^2$
				$(Q_{liq})^2$

parameters appears in the four models. Finally, the liquid flow Q_{liq} only affects the current density related to corrosion.

4.1. *Empirical models related to corroded mass*

Three responses were modelled in this study, namely the measured mass, the mass calculated by the analytical model and the difference between these two masses. For each empirical quadratic model, all the Echip6 statistical tests offered by Echip6 were successful. All the models presented hereafter are excellent from a statistical point of view. For each response, the adjusted correlation coefficient is greater than 0.95 and the model is predicative. The different polynomial models obtained after the refining process (both responses are expressed in grams for convenience) are as follows:

$$\begin{aligned} m_{meas} = {} & 0.0559 + 11.4456\,([Ce] - 7.5 \times 10^{-3}) \\ & + 0.01214\,(\ln[O_3] - \ln 0.24) \\ & + 0.0041\,(\ln[O_3] - \ln 0.24)^2 \end{aligned} \tag{21}$$

$$\begin{aligned} m_{calc} = {} & 0.00055 + 0.08163\,([Ce] - 7.5 \times 10^{-3}) \\ & + 7.95451(Q_{liq} - 30) \end{aligned} \tag{22}$$

The two models are surprisingly different. Moreover, they do not depend on the same hydrodynamic parameters. The measured mass depends on ozone flow but not on solution flow and vice versa for the calculated mass. Both models acknowledge cerium concentration as the most influent parameter, but the magnitude of the coefficients is quite different for each model. The constant of the empirical model represents the response value at the centre of the domain. A comparison between Equations 21 and 22 shows that the measured mass loss is 100 times greater than the calculated one.

A careful check proves that the difference is not due to a model or computational error. In fact this very puzzling result can be easily explained. The grain loosing effect was observed during certain experiments but the grain mass was not precisely quantified. Although the mass of grains is small at the reactor scale, it has a strong effect at the 10 micrometre layer scale. The mass difference can thus be attributed to the grain loosing effect that was not taken into account in the analytical model.

SEM micrographs (Part I) show that the grain diameter was close to 10 micrometres, which is precisely the thickness of the thin layer to be removed. The loosing effect (previously greatly underestimated) was identified through comparison between the two models. Grain detachment was due to cerium attack and appears as the most prominent agent of the overall corrosion process. Cerium thus enhanced the corrosion effect by a factor of 20 due to grain detachment. This result confirms the observations obtained from beaker experiments (Part I, Section 4.1).

The surface of the grains accounted for the largest part of Ce^{4+} consumption while the grains remained in the solution. This effect had a negative impact on the corrosion yields. The grains must therefore be filtered and continuously extracted from solution in the future industrial process.

Comparison of these two empirical models shows the limits of the first analytical model. The latter perfectly describes the first corrosion step (cerium attack) but does not take into account the second step (grain detachment effect), which appears to play a predominant role in the overall corrosion process. To conclude, the corrosion process involves two successive steps: (a) first, *the Ce^{4+} ions unseal the grains by specific intergranular attack*. This effect is probably well described by the analytical model presented in Section 3.1; (b) secondly, *the grains are detached and fall from the surface*. Only the empirical model takes account of both steps. This example illustrates one of the numerous advantages of empirical modelling which includes all the physical phenomena, even those unknown or hard to explain or model.

4.2. *Empirical model of the overall corrosion rate*

This model is required to design an efficient future industrial reactor. The corrosion rate v_{corr} is related to the corroded layer thickness Δe and the mass lost by corrosion Δm during time t:

$$v_{corr} = \frac{\Delta e}{t} = \frac{\Delta m}{\rho S t} \tag{23}$$

This response was deduced from the measured mass. After multilinear regression of experimental data and model refining, the corrosion rate is written as

$$\begin{aligned} v_{corr} = {} & 0.0578 + 12.888\,([Ce] - 7.5 \times 10^{-3}) \\ & + 0.0133\,(\ln[O_3] - \ln 0.24) \\ & + 0.0042\,(\ln[O_3] - \ln 0.24)^2 \end{aligned} \tag{24}$$

Here, v_{corr} is expressed for convenience in micrometres per hour. A 0.91 adjusted correlation coefficient for 15 degrees of freedom shows that the fit is good. The 0.006 experimental error SD computed from the five replicates gives a good idea of the precision of measurements. The normal plot (Figure 2) is linear and attests to the normality of residuals. The model is thus predictive and sufficiently precise for use in designing the future reactor.

Figure 3 presents a typical 3D plot of the corrosion rate response versus the two most influent parameters, namely the ozone flow logarithm (LO3) and the cerium concentration (Ce). The associated 2D contour plot given by Echip6 is given in Figure 4. Maximization of this fundamental response inside the convex hull (the area delimited by the experimental domain) gives a 0.144 ± 0.025 $\mu m\ h^{-1}$ optimal corrosion rate. This

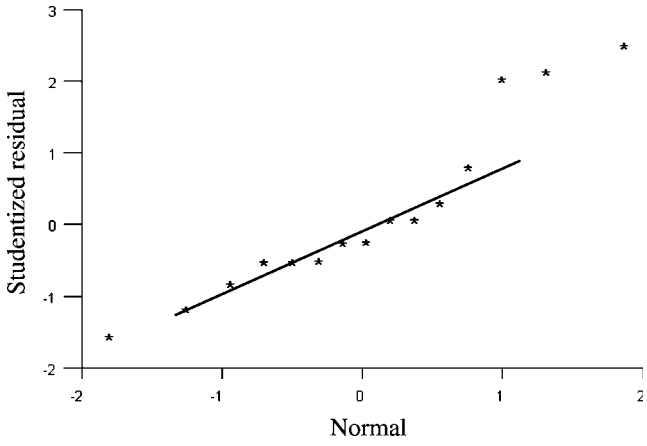

Fig. 2. Normal probability plot.

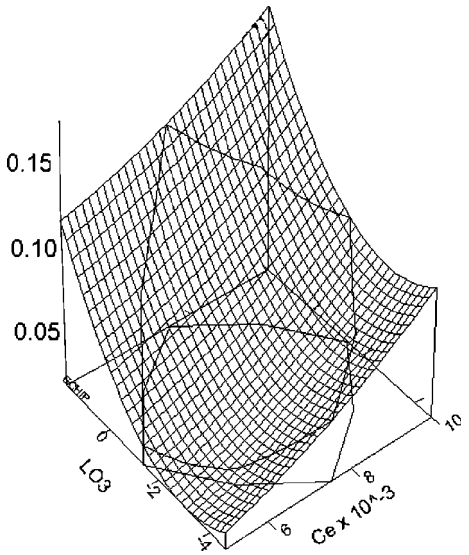

Fig. 3. 3D contour plot for corrosion rate. $Q_{liq} = 30$.

result was obtained for an ozone flow rate of 6 g h^{-1}, total cerium concentration of 7.5×10^{-3} mol l^{-1}, and a liquid flow rate of 30 l h^{-1}.

This 3.36 μm day^{-1} optimal rate is lower than the 10 μm day^{-1} rate imposed as an initial target. To reach such a target, it would be necessary to significantly increase the ozone flow rate (Note that the flow rate acts by its logarithm LO3 in Figure 4). This was not possible with the present apparatus, but could be easily achieved in a larger reactor.

4.3. *Empirical model of metal–solution potential difference*

Using the same approach as described previously, the refined empirical model of potential difference D_{dp} expressed in volt may be written as

$$D_{dp} = 0.3009 + 0.0113\,(\ln[O_3] - \ln 0.24) + 0.0026\,(\ln[O_3] - \ln 0.24)^2 \quad (25)$$

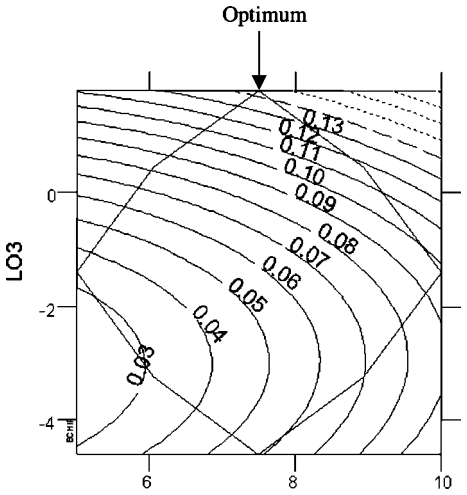

Fig. 4. Optimal corrosion rate on 2D contour plots. $Q_{liq} = 30$.

The experimental SD is as low as 0.0076, the adjusted correlation coefficient equals 0.888 and all the statistical tests are satisfied. The model is also a good predictive one. The theoretical model of Equation 17 shows that the potential difference between solution and metal depends only on Ce^{4+} concentration, at least in the experimental conditions. Thus, D_{dp} obviously depends in a nonlinear way on the regenerating ozone flow. This dependence explains the influence of cerium regeneration by ozone on the corrosion process.

4.4. *Model of corrosion current density*

The refined empirical model of corrosion current density gives

$$i_{cor} = 4.37858 \times 10^{-5} + 6.30676 \times 10^{-3} \times ([Ce] - 7.5 \times 10^{-3}) + 5.948 \times 10^{-7}(Q_{liq} - 30) + 2.75748 \times 10^{-8}(Q_{liq}^2 - 30^2) \quad (26)$$

This is an excellent model ($R_{squared} = 0.966$, $R_{adjust} = 0.959$, residual SD = 0.000002). In this model, corrosion current density depends only on cerium concentration and liquid flow.

The Pareto effect graph given by Echip6 (Figure 5) shows that the total cerium concentration is the most influential factor affecting corrosion current density within the experimental domain. The latter observation corresponds exactly to the physics of the problem. The liquid flow has a minor influence on current density, confirming the hypothesis of laminar flow.

To conclude, the numerical model of corrosion current density was validated by the DOE results and can be used to predict the corrosion rate of AISI 304 L by Ce^{4+}. It provides optimal operating and process control conditions through the use of the potential and ozone flow measurements.

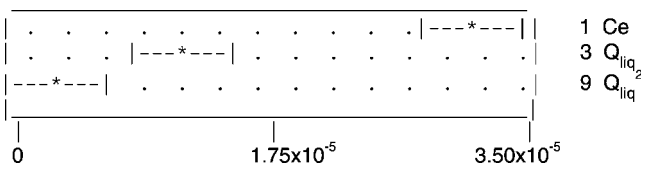

Fig. 5. Pareto effects graph for corrosion current.

5. Proposing a control method for an industrial reactor

We have shown in the previous paragraph that an ordinary electrode used to measure the potential in the reactor provides a low-cost, effective sensor. The corroded material mass and the corrosion rate can be computed before any experiment with Equations 13 and 17. When the total cerium content and the flow parameters are computed, a non-corrosive electrode is used to monitor the solution potential on-line. This measurement allows the calculation of mean corrosion current density. The difference between the result and the target value is used to compute the correction of ozone flow for optimal control of the corrosion process. This process is efficient, although the use of ozone requires some safety precautions. Nevertheless, cerium regeneration could also be obtained electrochemically [8].

6. Conclusions

The AISI 304 L alloy corrosion rate monitored by gravimetry was modelled as a function of total cerium concentration and ozone flow injected in the reactor. This empirical model takes into account all the parameters. Many of these parameters are hard to evaluate, such as the quantity of alloy grains that become detached from the metal by intergranular corrosion and fall into the dead zones of reactor. The empirical models provided evidence of a two-step corrosion process. Both the quantity and the dimensions of the grains falling into the liquid were at first underestimated. To ensure optimum efficiency, the grains will have to be extracted continuously from the recycled liquid flow in the future industrial reactor. The discrepancy between the effective measured mass of lost metal and the calculated corroded mass emphasised the limits of a theoretical model in this particular case.

The combined use of an empirical model obtained with DOE methodology and an analytical model of the corrosion rate was very efficient and provided a better understanding of the process and of performance optimization. The empirical model gives a precise description of corrosion current density. A simple precious metal electrode can be used as a low-cost, precise sensor providing a simple, effective control method for the future industrial reactor.

The decontamination process using ozone and cerium is perfectly in line with the strict requirements of the nuclear industry. Such a process does not require large investments in reactor engineering, monitoring and process control. Moreover, it may be applied to other materials such as AISI 316L alloy, commonly used in the nuclear industry.

References

1. F. Coeuret and A. Storck, 'Eléments de Génie Electrochimique', Technique et Documentation (Lavoisier, Paris, 2nd edn, 1993).
2. I. Rousar, K. Micka and A. Kimla, 'Electrochemical Engineering', Vols. 1 and 2 (Elsevier, Oxford, 1986).
3. G.E.P. Box and N.R. Draper, 'Empirical Model-building and Surface Responses' (J. Wiley & Sons, New York, 1987).
4. ECHIP6, 724 Yorklyn Road, Hockessin, DE 19707-8703, USA.
5. A.J. Bard and L.R. Faulkner, 'Electrochemical Methods. Fundamentals and applications' (J. Wiley & Sons, New York, 1980).
6. C.E. Harrington, *Ind. Qual. Contr.* **21** (10) (1965) 494.
7. J. Sacks, S.B. Schiller and W.J. Welch, *Technometrics* **31**(1) (1989) 41.
8. Y. Maeda, K. Sato, R. Ramaraj, T.N. Rao, D.A. Tryk and A. Fujishima, *Electrochim. Acta* **44** (1999) 3441.